CONVERGENCE ANALYSIS AND UPPER BOUND PROPERTY OF NS-RPIM WITH PURE RBFS USING VORONOI SMOOTHING DOMAINS

SIQING LI[*1,2], MING LI[1], AND G. R. LIU[1,3]

[1]Department of Mathematics, Taiyuan University of Technology, Shanxi, China
[2]Department of Mathematics, Hong Kong Baptist University, HongKong, China
[3]University of Cininnati, U.S.A.

ABSTRACT. In this paper, a nodal based smoothed point interpolation method (NS-RPIM) is implemented using Voronoi smoothing domains to solve elliptic partial differential equations with different node selection strategies. Shape functions for field variable approximation are built using the radial point interpolation method (RPIM) with pure radial basis functions (RBFs) without polynomial basis. The smoothed Galerkin weak form is applied to construct the discretized system equations. Triangle background cells with voronio smoothing domains and quadrilateral mesh with smoothing domains of equally-shared areas are used. It is found that in all cases that the NS-RPIM provides results with higher convergency rates for distorted mesh compared with the standard FEM. In addition, in all numerical examples, solutions for the energy norm by NS-RPIM are found to be upper bounds with respect to the FEM counterparts and even to exact solutions. In terms of accuracy, however, NS-RPIM could be more or less accurate than that of FEM dependent on the problem.

Keywords: Meshfree method; Radial point interpolation method (RPIM); smoothed Galerkin weak form; voronio smoothing domain, Node based smoothed radial point interpolation method (NS-RPIM)

AMS (MOS) Subject Classification. 39A10.

1. Introduction

Many problems in engineering can be well modeled in the form of partial differential equations (PDEs) in mathematics. It is well known that the Finite Difference method (FDM) [1,2,3] and Finite element method (FEM) [4,5,7] are widely used to solve PDEs. The mathematical theories of FEM are studied [6,7]. The fully compatible FEM based on the standard Galerkin weak form is overly-stiff, inaccuracy in stress solutions and high reliance on quality quadrilateral mesh [7]. Recently meshfree methods [8–14] offer attractive alternatives to the FEM for many problems using weak or weaked weak (W2) formulations. Some meshfree methods, like Kansas Method [27,28], use strong form collocation to discretize PDEs. In many meshfree methods,

the integration is still necessary. A strain smoothing technique was proposed by Chen [15] to stabilize the nodal integration process. Based on the strain smoothing technique, a generalized gradient smoothing (GGS) technique [31] was proposed for discontinuous nodal shape functions. By combining the Galerkin weak form and the GGS, Liu's team proposed the smoothed Galerkin weak form [19–23] for different engineering problems, including solid mechanics, heat transfer, acoustic problems. Based on the smoothed Galerkin weak form, there formed a series of numerical methods which can effectively produce solutions of nice properties. For example, cell-based smoothed finite element method that use FEM continuous shape functions (CS-FEM) has volumetric locking free property [19] and edge based smoothed point interpolation method (ES-PIM) has ultra-accurate property [25]. The node based smoothed finite element methods (NS-FEM) and node based smoothed point interpolation methods (NS-PIM) can obtain the softening effects and upper bound solutions [20,22,23,24]. Because more nodes can be used for shape functions construction, it can offer additional flexibility in formulation and can deliver much better solution in the NS-PIM method. However, approximated functions are generally no longer continuous in the domain. Therefore, fundamental changes in theory are required for these kinds numerical methods, which leads to the so-called G space theory [17–18]. The G space is a discrete space and does not require differentiable operations. And functions in G space are allowed certain discontinuity. It has been proved that solutions obtained by NS-PIMs are in G space and have many nice properties like softer, spatially stable, higher convergence in energy norm solutions than the FEM. Furthermore, they can provide super-convergent solution in the strain energy for solid mechanics problems governed by elliptic PDEs [26]. A more comprehensive review can be found in [32].

In this paper, the NS-RPIM is applied to solve elliptic partial differential equations. Radial basis functions (RBFs) and local support nodes are used to construct nodal shape functions by point interpolation Method (PIM). Nodal shape functions are called RPIM shape functions. They have the delta function property which allows straightforward imposition of essential boundary conditions. Support-node selection strategies based on triangle background cells and quadrilateral background cells are also introduced in the paper. Two approaches are used to constructing smoothing domains based on background cells, which are equally-shared area approach for quadrilateral background cells and Voronoi smoothing domains for triangle background cells. Equally-shared areas are constructed by connecting segments' midpoints and central points of quadrilateral background cells. Solutions obtained by NS-RPIM are not sensitive to mesh distortion. Therefore, we can obtain results with desired accuracy when problem domains are not regular and NS-RPIM is very promising in dealing with large deformation problems in engineering. Convergency behaviors of numerical solutions are studied in different irregular meshes. Another important property of

the NS-RPIM is that it can obtain upper bound solutions in energy norms than that of exact ones. We know that FEM method can have lower bound solutions in energy norm since it is a stiff model. Combing properties of energy norms solutions of FEM with that of NS-RPIM, we can estimated the exact solution in energy norm when it cannot be obtained.

This paper contains five sections. The Section 2 introduces the setting of the problems, governing PDEs and the construction of the nodal shape functions by the RPIM. We also introduce two node selection strategies based on background cells . In Section 3, equally shared smoothing domains and Voronoi smoothing domains are constructed based on background cells. We then brief the smoothed Galerkin weak form, discretion system by NS-RPIN based on the GGS technique, the G space theory and the smoothed Galerkin weak form. In Section 4, the numerical experiments are tested to show convergency behaviors with distorted meshes and the upper bound properties. We sum some concluding remarks in Section 5.

2. **Functions approximation using Point Interpolation Method (RPIM)**

In this paper, we consider the Possion Equations with both Dirichlet and Numman boundary conditions imposed on the boundary as:

$$\mathcal{L}u = f \quad \text{in } \Omega \tag{2.1}$$

$$u|_{\Gamma_1} = g_1 \tag{2.2}$$

$$\frac{\partial u}{\partial \mathbf{n}}|_{\Gamma_2} = g_2 \tag{2.3}$$

where $\mathcal{L}u = -\sum_{i=1}^{d} a_{ii}\partial_{ii}u$ is the elliptic operator and Ω is a domain in $\mathbb{R}^d$, Γ_1, Γ_2 is subset of boundary $\partial\Omega$ which satisfy $\Gamma_1 \cup \Gamma_2 = \partial\Omega$. Scattered node set $X = \{\mathbf{x}_1, \ldots, \mathbf{x}_{N_n}\}$ are arbitrarily given in the domain Ω and on the boundary $\partial\Omega$. Nodal basis functions $\phi_i(x)$, $i = 1, 2, \ldots, N_n$ are needed to approximate the numerical solution. Unlike the Finite Element Method (FEM) which uses polynomial basis functions to develop nodal basis functions, we use pure RBFs in this paper:

$$\phi_i(\mathbf{x}) = \phi_i(r) \quad i = 1, 2, \ldots, N_n$$

where $r = \|x - x_i\|_2$ is the Euclidean norm in $\mathbb{R}^d$ of difference between point $\mathbf{x}$ and the ith node $\mathbf{x}_i$. It should be noted that no polynomial basis are used. Then numerical solution u^h at any point $x \in \mathbb{R}^d$ can be approximated by RBFs using local support nodes:

$$u^h(\mathbf{x}) = \sum_{i=1}^{N_s} \phi_i(\mathbf{x})a_i = \mathbf{\Phi}^T(\mathbf{x})\mathbf{a} \tag{2.4}$$

where a_i, $i = 1, 2, \ldots, N_s$ are unknown coefficients and vector $\mathbf{a}^T(\mathbf{x}) = [a_1, a_2, \ldots, a_n]$, N_s is the number of local support nodes of x, ϕ_i, $i = 1, 2, \ldots, N_s$ are the basis of supports nodes which can be determined in the node selection part.

2.1. **Nodal Shape Functions by RPIM.** Nodal shape functions are constructed by the radial point interpolation method (RPIM), which forces the approximated function passing through all the local support nodes. We have the following conditions:

$$(2.5) \qquad u_k = u^h(\mathbf{x_k}) = \sum_{i=1}^{N_s} \phi_i(\mathbf{x_k}) a_i \quad k = 1, 2, \ldots, N_s$$

and in matrix form, it becomes

$$\mathbf{u_s} = \mathbf{\Theta}_s \mathbf{a}$$

in which $\mathbf{u_s} = [u_1, u_2, \ldots, u_{N_s}]$ is the vector collecting all function values at the N_s local support nodes, $\mathbf{\Theta}_s$ is the square moment interpolate matrix with RBFs evaluated on the local nodes:

$$\mathbf{\Theta}_s = \begin{pmatrix} \phi_1(\mathbf{x}_1) & \phi_2(\mathbf{x}_1) & \cdots & \phi_n(\mathbf{x}_1) \\ \phi_1(\mathbf{x}_2) & \phi_2(\mathbf{x}_2) & \cdots & \phi_n(\mathbf{x}_2) \\ \cdots & & & \\ \phi_1(\mathbf{x}_n) & \phi_2(\mathbf{x}_n) & \cdots & \phi_n(\mathbf{x}_n) \end{pmatrix}.$$

It has been proved that matrix $\mathbf{\Theta}_s$ is always invertible for scattered nodes. Therefore, we can calculate the coefficient vector $\mathbf{a}$ as

$$\mathbf{a} = \mathbf{\Theta}_s^{-1} \mathbf{u_s}.$$

Substituting the value of $\mathbf{a}$ to Eq. 2.4, we have:

$$(2.6) \qquad u^h(\mathbf{x}) = \mathbf{\Psi}_s(\mathbf{x}) \mathbf{u_s}^T$$

where $\mathbf{\Psi}_s(\mathbf{x})$ is the row matrix of nodal shape functions of the N_s support nodes:

$$(2.7) \qquad \mathbf{\Psi}_s = \mathbf{\Theta}\mathbf{\Theta}_s^{-1} = [\psi_1(\mathbf{x}) \quad \psi_2(\mathbf{x}) \cdots \psi_{N_s}(\mathbf{x})]$$

Based on the above RPIM construction process, RPIM nodal shape functions possess the Delta function property [14]

$$\phi_i(\mathbf{x}_j) = \begin{cases} 1 & \text{when } i = j, \\ 0 & \text{when } i \neq j \end{cases}$$

in which $\mathbf{x}_j$ is coordinates of jth node. This property allows easy treatment for essential conditions at the boundary node. However, differences in nodal shape functions of FEM, RPIM shape functions are constructed by using the support nodes. Therefore, it may not continuous at points where support nodes are updated. In FEM [7], we generally need coordinate mapping to ensure the continuity. The RPIM method

(a) (b)
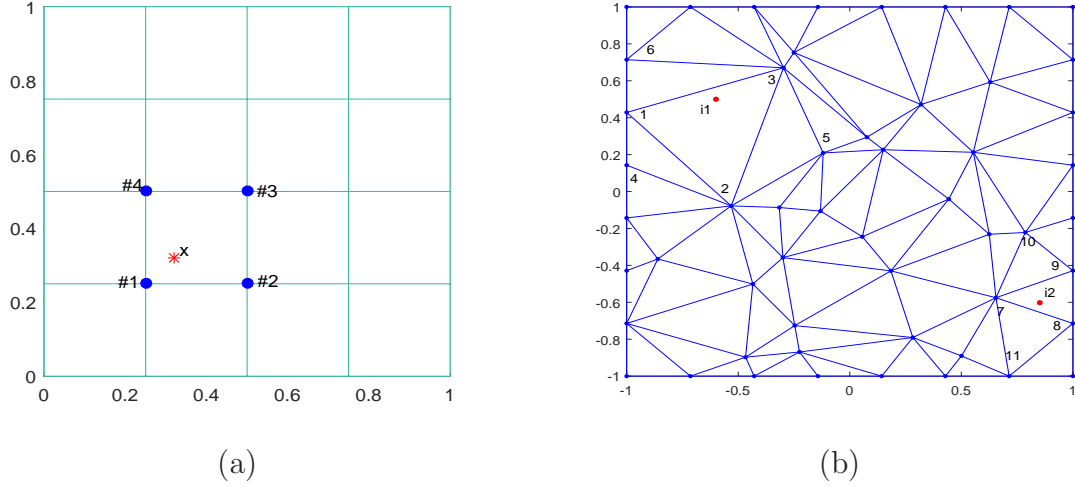
FIGURE 1. Quadrilateral(a) and Triangular(b) Background cells and support node selection

is straightforward and do not need mapping, because G space theory allows the use of discontinuous functions.

When constructing the RPIM nodal shape functions, we need to select the support nodes of the interest point x, for which background cells are useful. Numerical integration also needs background cells. In 2D problems, triangular cells (T3) and quadrilateral cells (Q4) which are nonoverlapping and seamless (i.e $\Omega = \sum_{k=1}^{N_c} \Omega_k^c$ and $\Omega_i^c \bigcap \Omega_j^c = \emptyset, i \neq j$) are mostly used in FEM. In this work, these two kinds background cells are used to select the support nodes. When use quadrilateral cells (Q4), for an point x of interest, we choose four nodes $(1, 2, 3, 4)$ of the element that hosts the point x in Figure 1. For triangular cells (T3) hosting $i1$, we choose three nodes $(1, 2, 3)$ of the element and three nodes $(4, 5, 6)$ of the neighbouring elements which share the same edge with the element. For points belongs the boundary element, based on the same selection strategy, four or five support nodes will be selected, as show in Figure 1.

3. The Smoothed Galerkin Weak form and Dicretized System Equations

3.1. **Node Based Smoothing Domains.** Based on the above support node selection strategies, the shape functions are discontinuous on the boundary of background cells. The GGS is needed to define the inner product of shape functions, so they can belongs to a G_h^1 space, for which a set of smoothing domains are required. The problem domain Ω is further divided into N_n node based smoothing domains which must satisfy two conditions: 1. $\Omega = \sum_{k=1}^{N_n} \Omega_k^s$ and $\Omega_i^s \bigcap \Omega_j^s = \emptyset, i \neq j$, i.e nonoverlapping, no gap and each smoothed domain contains only one node; 2. The boundary of the each smoothed domain $\Gamma_i^s, i = 1, 2, \ldots, N_n$ should satisfy the "no-sharing rule": Γ_i^s,

(a)   (b)
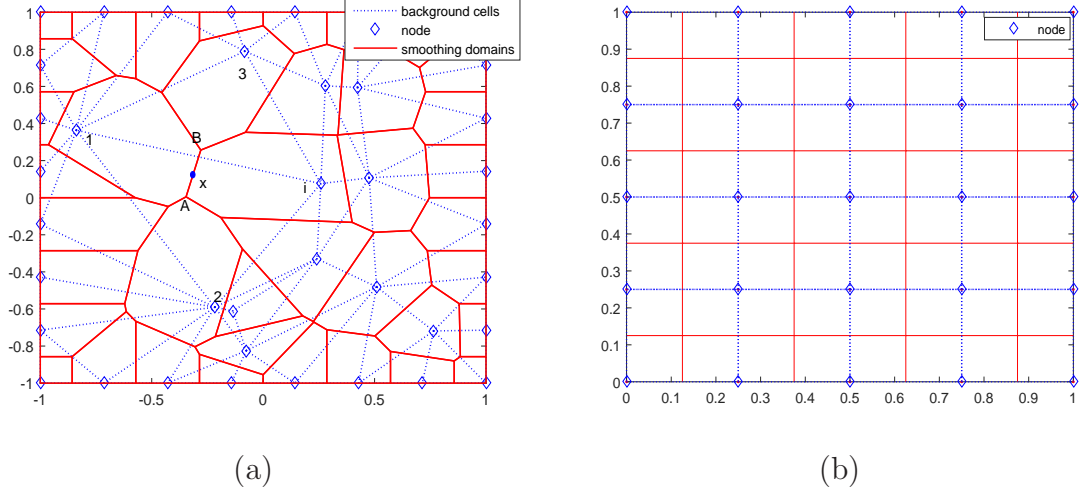
FIGURE 2. Voronoi (a)and Equally Shared (b) Smoothing Domain:
Smoothing Domain: red polygon; Background cell: blue polygon

$i = 1, 2, \ldots, N_n$ should not share any finite portion of the lines on which the function is not square integrable. Two kinds node based smoothing domains are used in our work: equally-shared smoothing domains and the Voronoi smoothing domains, as show in Figure 1(a) and Figure 1(b).For quadrilateral background cells(Q4), we use equally-shared smoothing domains which are generated by connecting sequentially the mid-edge points to the central point of the adjoint background quadrilaterals sharing the node. Voronoi smoothing domains associated with the nodes are built by using the standard Voronoi diagram based on the triangle background cells. Figure 2 shows these two kinds smoothing domains.

Based on the Voronoi smoothing domains and triangle background cells, we introduce another node selection strategy. Functions at a point located on boundary of Vorinoi smoothing domain segment Γ_i^s is approximated using nodes of the triangles connected cut by Γ_i^s. For example, for any point $\mathbf{x}$ on segment AB, four support nodes $1, 2, i, 3$ are selected (see in left part of Figure 2(b)).

3.2. **The Smoothed Galerkin weak Form.** Based on the argument in [14], if function u, W are both continuously differentiable at the closure of Ω_i^s, then the derivative of u has the following integral representation:

$$(3.1) \qquad \frac{\partial u}{\partial x_j}(\mathbf{x}) = \int_{\Omega_i^s} \frac{\partial u(\xi)}{\partial x_j} W(\mathbf{x} - \xi) d\xi \quad j = 1, 2, \ldots, d, \quad i = 1, 2, \ldots, N_n$$

then by the Green's theorem, we can obtain:

$$\frac{\partial u}{\partial x_j}(\mathbf{x}) = \int_{\Gamma_i^s} u(\xi) n_j W(\mathbf{x} - \xi) d\xi$$

$$(3.2) \qquad - \int_{\Omega_i^s} u(\xi) \frac{\partial W(\mathbf{x} - \xi)}{\partial x_j} d\xi \quad j = 1, \ldots, d, \ i = 1, \ldots, N_n$$

where n_j is the *jth* component of the unit outer normal vector $\mathbf{n}$ on Γ_i^s and W is the smoothing function. For simplicity, we use the Heaviside smoothing function in this paper which is

$$W(\mathbf{x} - \xi) = \begin{cases} \frac{1}{A_i^s} & \text{when } \mathbf{x} \in \Omega_i^s, \\ 0 & \text{Otherwise.} \end{cases}$$

where A_i^s is the area of the smoothing domain Ω_i^s. Then we can approximate the derivative of function u as

$$(3.3) \qquad \frac{\partial u}{\partial x_j}(\mathbf{x}) \approx \frac{\bar{\partial} u}{\partial x_j}(\mathbf{x}) = \frac{1}{A_i^s} \int_{\Gamma_i^s} u(\xi) n_j d\xi \quad j = 1, \ldots, d, \ i = 1, \ldots, N_n.$$

Because of the shape construction process and two node selection strategies given in Section 2 and Section 3, the approximated solution u^h in Eq. 2.5 have only finite discontinuous points on the boundary of smoothing domains, Eq. 3.3 can be used to approximate the derivative of the numerical solution for both kinds of smoothing domains.

The smoothed Galerkin weak form (weakend weak form) for the PDE becomes [14]:

$$(3.4) \qquad \sum_{i=1}^{N_n} \left(A_i^s \left(\sum_{j=1}^{d} \int_{\Gamma_i^s} v n_j d\xi \int_{\Gamma_i^s} u n_j d\xi \right) \right) = \sum_{i=1}^{N_n} \left(\int_{\Omega_i^s} f v d\xi + \int_{\Gamma_2} g v d\xi \right)$$

Our numerical solution will be obtained based on the above smoothed Galerkin weak form. It is obviously seen form Eq. 3.4 that we do not need u, v in H^1 space any more, because we do not require derivatives of the functions. They need to be in the following G^s space [30]:

$$G^s(\Omega) = \left\{ \begin{array}{l} f(\mathbf{x}) \in L^2(\Omega) \\ \sum_{i=1}^{N_s} \frac{1}{A_i^s} \left| \int_{\Gamma_i^s} f(\mathbf{x}) \mathbf{n_i} d\mathbf{x} \right|^2 \text{ is bounded on } \Omega \ \langle 1 \rangle \\ \sum_{i=1}^{N_s} \frac{1}{A_i^s} \left| \int_{\Gamma_i^s} f(\mathbf{x}) \mathbf{n_i} d\mathbf{x} \right|^2 = 0, \text{ iff } f(\mathbf{x}) \equiv c \, (c \text{ is any constant}) \ \langle 2 \rangle \end{array} \right\}$$

where n_i is the outer vector on the boundary Γ_i^s of smoothing domain Ω_i^s.

Proposition 3.1 (Upper bound property of NS-RPIM [29]). *The solution in energy form for the PDE is defined as*

$$U_e = \frac{1}{2} \int_{\Omega} (\nabla u)^T (\nabla u) d\Omega.$$

The NS-RPIM solutions in energy norm has the following property

$$\overline{U_e}(\overline{\mathbf{u}}) \geq U_e \geq \overline{U_e}(\widetilde{\mathbf{u}})$$

where $\overline{U_e}(\overline{\mathbf{u}})$ is the numerical solution in strain energy by NS-RPIM, U_e is that of the exact solution and $\overline{U_e}(\widetilde{\mathbf{u}})$ is that of the numerical solution by compatible FEM.

3.3. **Discrete System of NS-RPIM.** Functions u, v in G_h^1 space can be approximated by nodal shape functions and corresponding nodal values. For any $x \in \Omega$ [14],

$$(3.5) \qquad u(\mathbf{x}) = \mathbf{\Psi}_s(\mathbf{x})\mathbf{U_s}^T, \quad v(\mathbf{x}) = \mathbf{\Psi}_s(\mathbf{x})\mathbf{V_s}^T,$$

where $\mathbf{\Psi}_s$ is the matrix of RPIM shape function obtained using the support nodes of x, U_s and V_s are the function values of support nodes. Substituting above approximations to the smoothed Galerkin weak form Eq. 3.4 and write the formulation in matrix form, we can obtain the following discrete system

$$(3.6) \qquad \mathbf{KU}^T = \mathbf{F}$$

where $\mathbf{K}$ is matrix obtained from the integration term in Eq. 3.4, $\mathbf{U}$ is the vector of node value of function u and $\mathbf{F}$ is the vector of right hand side. They can be expressed as

$$(3.7) \qquad \mathbf{K} = \sum_{sd=1}^{N_n} A_i^s \mathbf{B}_s^T \mathbf{B}_s, \quad \mathbf{U} = [u_1, \ldots, u_{N_n}], \quad \mathbf{F} = \sum_{sd=1}^{N_n} \mathbf{F}_s^T.$$

where

$$(3.8) \qquad \mathbf{B}_s = [\mathbf{B}_{s,1}, \mathbf{B}_{s,2}, \ldots, \mathbf{B}_{s,N_s}], \text{ and } \mathbf{B}_{s,i} = [B_{s,i}^1, B_{s,i}^2, \ldots, B_{s,i}^d]^T$$

and by Gaussian integration on the boundary of each smoothing domain, we obtain

$$(3.9) \qquad \begin{aligned} B_{s,i}^j &= \int_{\Gamma_i^s} \psi_s^i(\mathbf{x}) n_j d\xi \\ &= \sum_{m=1}^{Nsg} \left(\sum_{n=1}^{Ng} \omega_n \psi_s^i(\mathbf{x}_{mn}) n_j(\mathbf{x}_{mn}) \right), \quad i = 1, \ldots, N_s, j = 1, \ldots, d. \end{aligned}$$

where Nsg is the number of the Γ_i^s and Ng is the number of Gauss points located each segment, ω_n is the weighting of the corresponding gauss point. For right hand side vector, by the same argument we have

$$\mathbf{F}_s = [F_{s,1}, F_{s,2}, \ldots, F_{s,N_s}], \text{ with}$$
$$(3.10) \qquad F_{s,i} = \int_{\Omega_i^s} f\psi_s^i(\mathbf{x})d\xi + \int_{\Gamma_2} g_2\psi_s^i(\mathbf{x})d\xi, \quad i = 1, \ldots, N_s.$$

Solving the linear system Eq. 3.4, we can obtain the nodal function values. The functions of the solution and there derivative can then easily obtained using the RPIM shape functions.

4. Numerical Experiments

In our numerical examples, Gaussian radial basis functions $\phi_i(\mathbf{x}) = e^{-\varepsilon^2 \|\mathbf{x}-\mathbf{x}_i\|^2}$, $i = 1, 2, \ldots, N_n$ are used for construct the nodal shape functions, where $\varepsilon > 0$ is the shape parameter. We use a numerically stable approach (RBF-QR) [33] to perform the Gaussian radial basis interpolation in the RPIM process. This RBF-QR can overcome the ill-condition of the matrix when shape parameter ε is small and can obtain more accurate solution.

In all numerical experiments, we compute the RMES error over the whole domain Ω:

$$E_r = \sqrt{\frac{\sum_{i=1}^{Nn}(u_i^* - \widetilde{u}_i)^2}{N_n}}$$

in which u^*, $\widetilde{u}_n$ are the analytic solution and the numerical solution obtained by NS-RPIM for the PDE respectively. To study the property of the presented NS-RPIM, we also compute the equivalent energy norm as an indicator of the error of the numerical scheme:

$$U_e = \frac{1}{2} \int_\Omega B^T B^B d\Omega = \begin{cases} \frac{1}{2}\sum_{i=1}^{N_s} A_i^s ((\overline{B}_i^s)^T \overline{B}_i^s) & \text{for NS-RPIM,} \\ \frac{1}{2}\sum_{j=1}^{N_e} A_j^e ((B_j^e)^T B_j^e) & \text{for FEM,} \end{cases}$$

where A_i^s, A_j^e, $i = 1, \ldots, N_S$, $j = 1, \ldots, N_e$ are areas of the smoothing domain for NS-RPIM and element for FEM respectively. Convergence rates of our numerical method is defined as

(4.1)
$$r = \ln\left(\frac{E_r^{h_1}}{E_r^{h_1}}\right) \setminus \ln\left(\frac{h_1}{h_2}\right)$$

where $E_r^{h_1}, E_r^{h_1}$ are the relative errors under two different characteristic length h_1, h_2 which defined as $h = \sqrt{\frac{A_\Omega}{N_e}}$ where A_Ω is the area of the whole problem domain, N_e is the number of background cells.

4.1. **Example 1.** We consider the first example which exact solution is $u(x,y) = \sin(x^2 + y^2)$ and the elliptic operator is $\mathcal{L} = -(\frac{\partial^2}{\partial x^2} + \frac{\partial^2}{\partial x^2})$. In this example, we use two kinds of background cells: quadrilateral and triangular background cells.

We use quadrilateral background cells in this example to show the performance of the method. When we consider the Q4 background cells, to analysis the influence of mesh distortion for our method, we add random disturbance by beta distribution to the location coordinates of the nodes which is

(4.2)
$$f(x) = \frac{\Gamma(\alpha+\beta)}{\Gamma(\alpha)\Gamma(\beta)} x^{\alpha+1}(1-x)^{\beta-1} \quad x \in (0,1)$$

where $\Gamma(\alpha), \Gamma(\beta)$ are Γ functions with α, β as distribution parameter. The distortion parameter is defined as:

$$Dt = \mu(2\epsilon - 1),$$
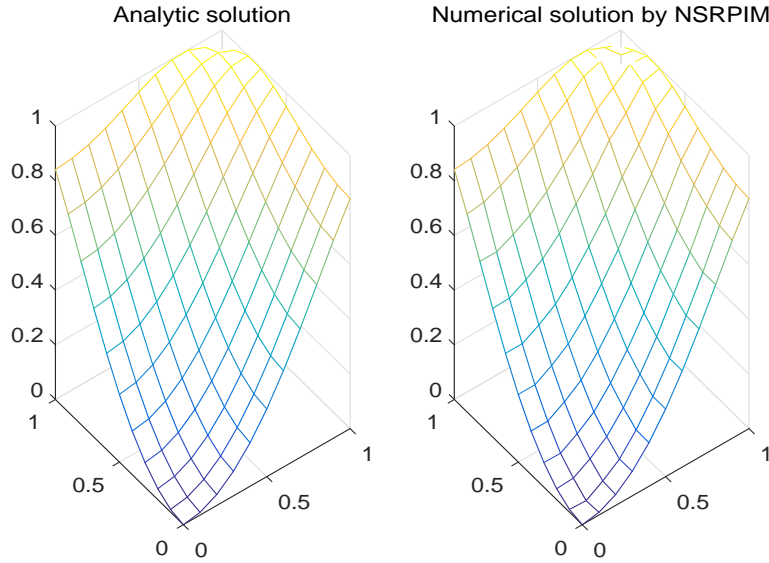
FIGURE 3. Analytic solution and numerical solution by NS-RPIM when 121 nodes are used.

in which $\mu \in [0,1]$ is the irregular factor and ϵ is a random number produced using beta distribution.

In this case, the problem domain is: $\Omega = [0,1] \times [0,1]$. Dirichlet boundary conditions are imposed on the boundary of domain $\partial\Omega = \Gamma_1 = \{x = 0, y \in [0,1]; x = 1, y \in [0,1]; y = 0, x \in [0,1]; y = 1, x \in [0,1]\}$. For NS-RPIM method, equally shared smoothing domains based on quadrilateral cells are used. For FEM, the quadrilateral elements are used. The exact energy norm in Ω is 0.5333. Figure 3 plots the analytic solution and numerical solution by NS-RPIM. Figure 4(a) is the RMES errors as node numbers increasing. From Figure 4(b), it can be seen that when background quadrilateral cells are not regular, the accuracy of numerical solution by FEM decrease dramatically. However, the errors by NS-RPIM are very stable and capped small. Hence, the NS-RPIM is resistance to mesh distortion. The table of Figure 5(a) lists the energy norms by FEM and NS-RPIM for different characteristic length of the mesh. In Figure 5(a), it can be obviously seen that NS-RPIM solutions are an upper bound to that of FEM. Figure 5(b) shows the convergence process of the numerical solutions. It can be seen that solutions by NS-RPIM provide upper bounds, and solutions by FEM provides lower bounds. They together bound the exact solution from two sides.

4.2. **Example 2.** In this example, we first study the convergency performance of the NS-RPIM. The domain and the elliptic operator is same as that for the Example 1. The analytic solution in this case is $u(x,y) = e^{x^2+y^2}$ and Dirichlet boundary conditions are imposed on the boundary. For quadrilateral background cells, Table 1 present the
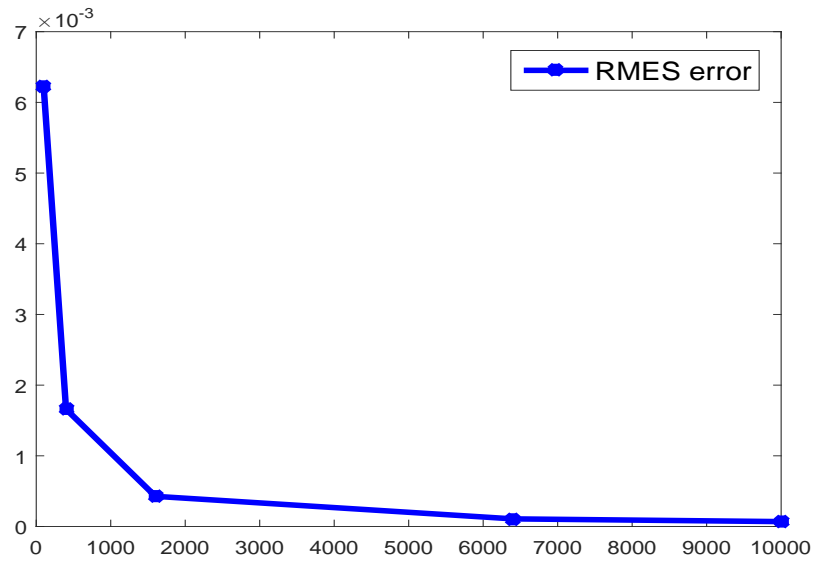
(a)
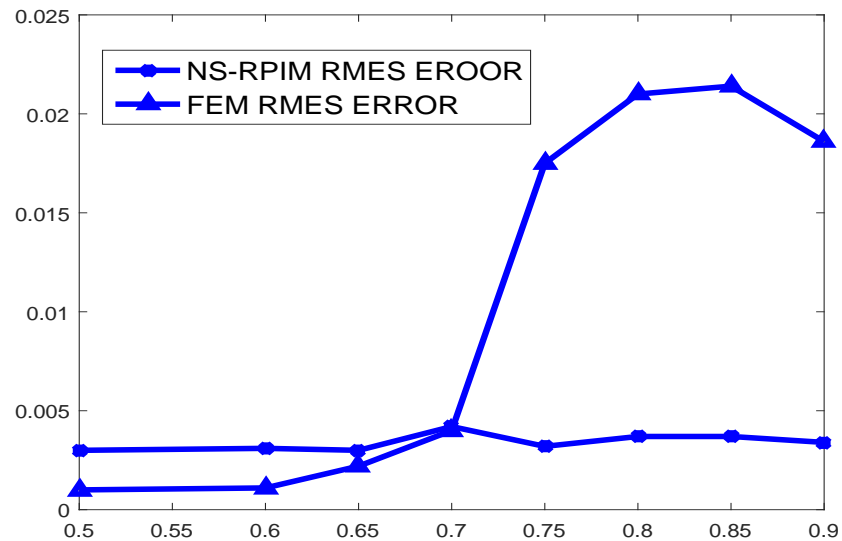
(b)

FIGURE 4. RMES errors as node number increasing(a) and RMES errors compared with FEM as mesh are not regular (b)

RSME errors when irregular factors are 0.6, 0.7 and 0.8, respectively, for different node numbers. It can also be seen that the numerical solutions by NS-RPIM in these two cases are more accurate than solutions by FEM. Here, we further evaluate relative convergency rate of NS-RPIM in comparison with FEM. Figure 6 presents the convergence curves when irregular factor from 0.5 to 0.9 and it shows that both convergency rates and accuracies of solutions by NS-RPIM are higher than that of

h	$En_{NS-RPIM}$	En_{Exact}	En_{FEM}
0.1	0.5352	0.5333	0.5294
0.05	0.5339	0.5333	0.5323
0.025	0.5335	0.5333	0.5331
0.0125	0.5334	0.5333	0.5332

(a)
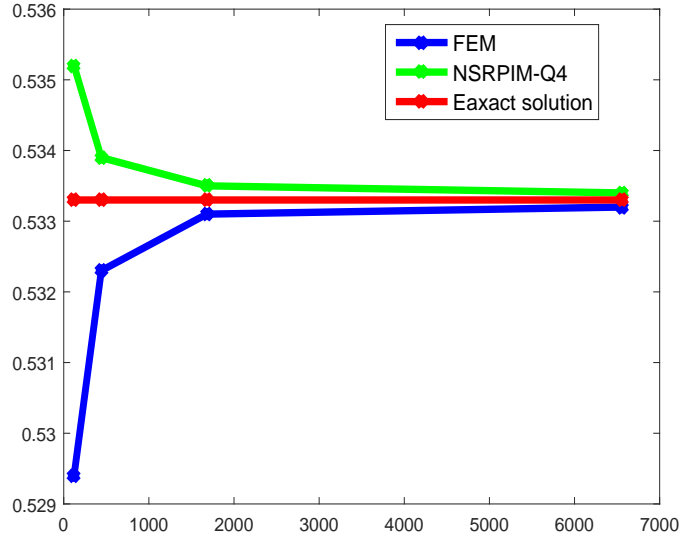
(b)

FIGURE 5. Energy Norms as character length decrease in Ex 1 for quadrilateral background cells

FEM when irregular factor is larger than 0.5. These results show again that the NS-RPIM is not sensitive to mesh distortion.

Next, we study the upper bound properties of NS-RPIM for different background cells and different kinds of smoothing domains. For quadrilateral background cells and equally shared smoothing domain in domain $\Omega_1 = \{(x,y) \in \mathbb{R}^2 | x \in [0,1], y \in [0,1]\}$, the exact solution in energy norm is 11.8804. Figure 7 shows the energy norms by NS-RPIM together with that of FEM. It is observed again that the energy norms by NS-RPIM is upper bounded solutions to both exact solutions and numerical solutions by FEM. For triangle background cells and voronoi smoothing domains in domain $\Omega = \{(x,y) \in \mathbb{R}^2 | x \in [-1,1], y \in [-1,1]\}$, the exact solution for energy norm is 47.5218. We use all-nodes-on-path selection strategy. Figure 8 is solutions in energy norms by NS-RPIM and that of FEM. It can be seen that energy solutions by NS-RPIM are upper bound solutions to exact solutions and energy norms by FEM are the lower bound solutions. We noted that in this example, the accuracy of NS-RPIM is lower than that of FEM counterpart.

TABLE 1. RMES errors by SRPIM in irregular mesh for EX2

Irregular factor	node number	RMES Errors of NS-RPIM	RMES Errors of FEM
	100	$8.6929 * 10^{-2}$	$9.2845 * 10^{-2}$
	400	$1.8416 * 10^{-2}$	$3.7186 * 10^{-2}$
0.6	900	$1.0007 * 10^{-2}$	$2.4114 * 10^{-2}$
	1600	$6.5816 * 10^{-3}$	$2.3374 * 10^{-2}$
	100	$5.3376 * 10^{-2}$	$5.3557 * 10^{-2}$
	400	$2.9277 * 10^{-2}$	$3.8827 * 10^{-2}$
0.7	900	$1.1572 * 10^{-2}$	$2.3926 * 10^{-2}$
	1600	$7.8882 * 10^{-3}$	$1.0104 * 10^{-2}$
	100	$7.9872 * 10^{-2}$	$9.0156 * 10^{-2}$
	400	$1.8967 * 10^{-2}$	$3.2993 * 10^{-2}$
0.8	900	$1.2868 * 10^{-2}$	$2.7812 * 10^{-2}$
	1600	$8.6827 * 10^{-3}$	$2.4967 * 10^{-2}$

TABLE 2. RMES errors of FEM and SRPIM for EX3

h	NS-RPIM	FEM
0.1	$2.43 * 10^{-3}$	$1.712 * 10^{-3}$
0.05	$9.9380 * 10^{-4}$	$6.4927 * 10^{-4}$
0.025	$3.7894 * 10^{-4}$	$2.3756 * 10^{-4}$
0.00625	$5.0433 * 10^{-5}$	$3.0454 * 10^{-5}$

4.3. **Example 3.** In this example, we consider the example with singular points in the problem domain. The exact solution is $u(x, y) = \sqrt{x + y}$ and we can easily computing the $\mathcal{L}u = -\Delta u = \frac{1}{2}\frac{1}{\sqrt{(x+y)^3}}$. It can be seen that point $(0, 0)$ is a singularity point on the boundary of problem domain at which both the first and second derivatives do not exist. Table 2 shows that our NS-RPIM can obtain numerical solutions which accuracy is same order with that of FEM even under the regular quadrilateral mesh. Figure 9 shows that convergency rates of the NS-RPIM are higher than that of FEM. Accuracies are in the same order and we can even obtain the better solution when background meshes are not regular. Figure 10 plots the absolute errors of FEM and NS-RPIM when characteristic length of mesh is 0.05. Table 3 is the numerical solutions when irregular factor changes from 0.6 to 0.8, it can be seen again that we can obtain more accurate and higher convergence rates when meshes are distortion.

5. **Conclusions**

In this implementation of NS-RPIM, we use pure radial basis functions for constructing RPIM shape functions and polynomial basis are not used. Triangle background cells with voronoi smoothing domains, and quadrilateral background cells
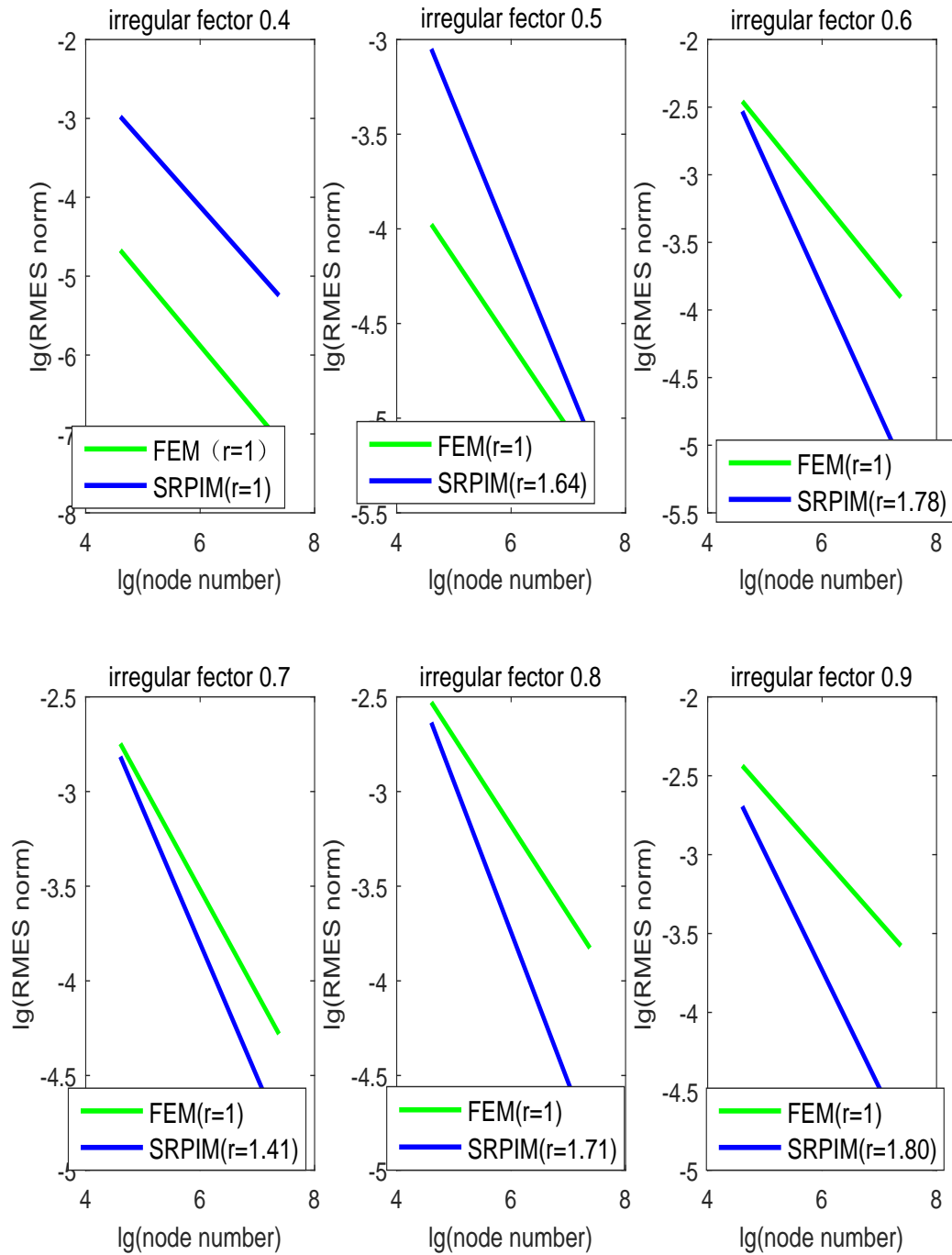
FIGURE 6. Convergency of EX3 for distortion meshes

with smoothing domains of equally share areas are applied to create our NS-RPIM models. We found that NS-RPIM results have higher convergency rates when compared the results by FEM using the same mesh. We also found that NS-RPIM is insensitive to mesh distortion. Thus this method is very promising in dealing with

h	En_{pim1}	En_{exact}	En_{fem1}
0.1	12.0730	11.8804	11.8552
0.05	11.9337	11.8804	11.8740
0.025	11.8940	11.8804	11.8788
0.0125	11.8838	11.8804	11.8800

(a)
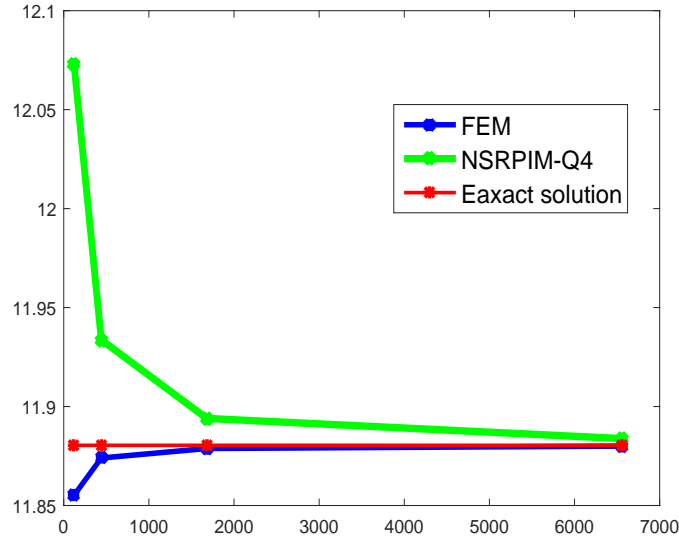
(b)

FIGURE 7. Energy Norms as character length decrease in Ex2 for quadrilateral background cells

TABLE 3. RMES errors by SRPIM in irregular mesh for EX3

irregular factor	node number	NS-RPIM error	FEM error
0.6	100	$5.4557 * 10^{-3}$	$2.4120 * 10^{-3}$
	400	$1.4338 * 10^{-3}$	$1.6315 * 10^{-3}$
	900	$1.1135 * 10^{-3}$	$1.5885 * 10^{-3}$
	1600	$7.0601 * 10^{-4}$	$8.8682 * 10^{-4}$
0.7	100	$6.0276 * 10^{-3}$	$4.8284 * 10^{-3}$
	400	$2.5590 * 10^{-3}$	$2.9642 * 10^{-3}$
	900	$1.1230 * 10^{-3}$	$1.3434 * 10^{-3}$
	1600	$7.7790 * 10^{-4}$	$8.8278 * 10^{-3}$
0.8	100	$4.3137 * 10^{-3}$	$5.3834 * 10^{-3}$
	400	$1.9565 * 10^{-3}$	$3.9094 * 10^{-3}$
	900	$1.3146 * 10^{-3}$	$3.2711 * 10^{-3}$
	1600	$6.9621 * 10^{-4}$	$1.1706 * 10^{-3}$

h	En_{fem}	U_{Exact}	En_{pim}
56	47.4424	47.5218	54.9589
196	47.4901	47.5218	50.8592
236	47.4888	47.5218	50.5012
326	47.4970	47.5218	49.9657

(a)
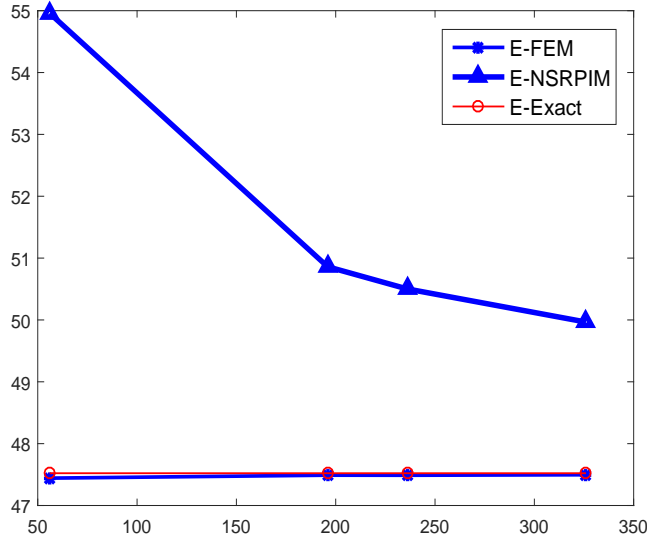
(b)

FIGURE 8. Energy Norms as character length decrease in Ex2 for Tri-angle background cells

large deformation problems. For solutions of energy norm, NS-RPIM provides upper bounds to the exact solution and, in contrast that the FEM can provides the lower bound solutions. Together, they can bound the exact solution from two sides for all problem we tested so far.

ACKNOWLEDGMENTS
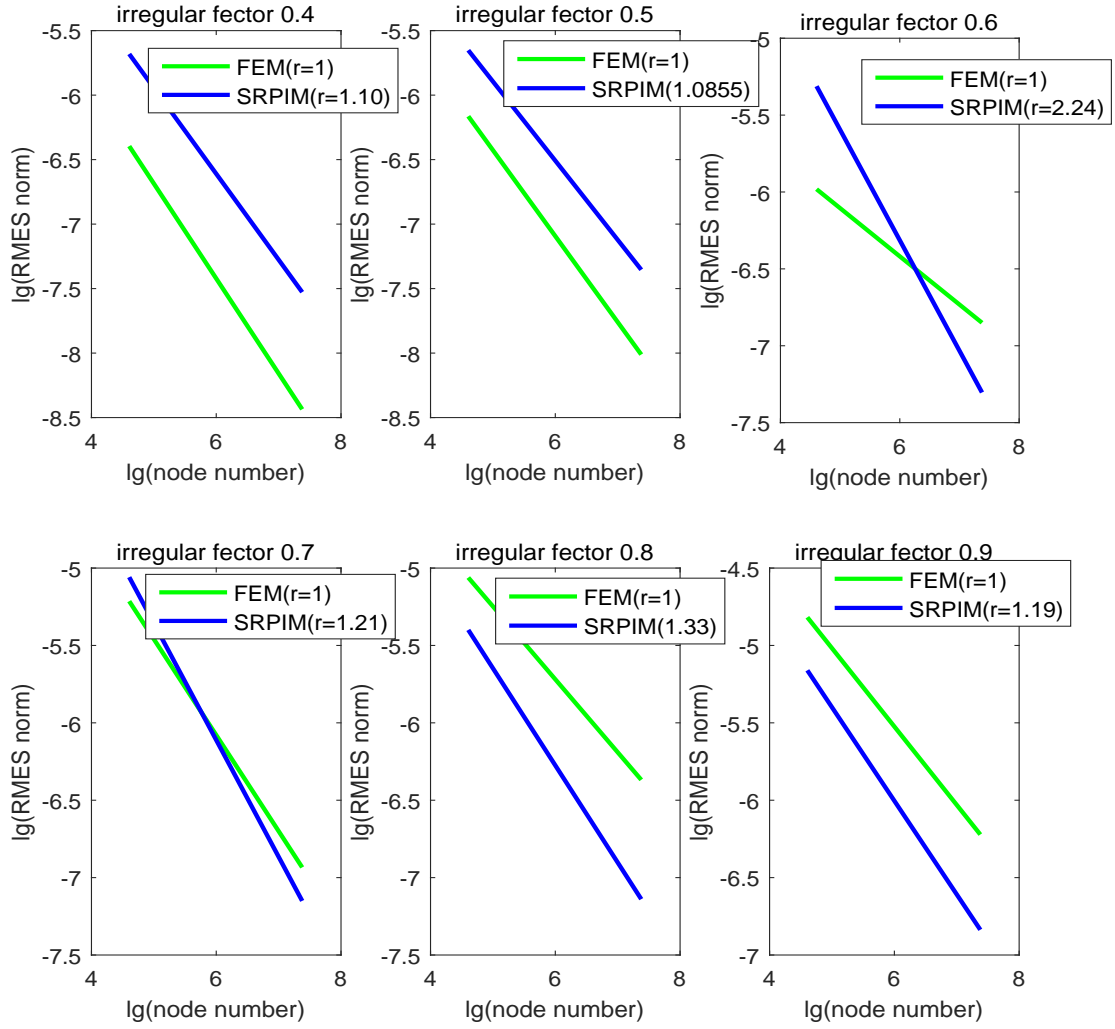
FIGURE 9. Convergency of EX3 for distortion meshes
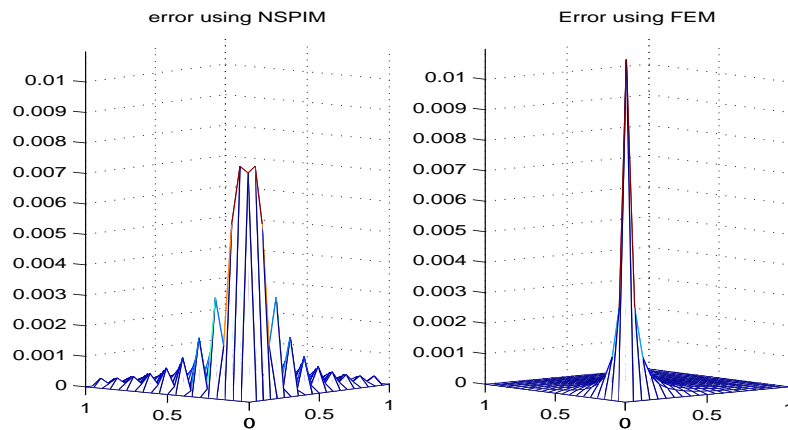
FIGURE 10. Absolute errors of FEM and NS-RPIM when mesh size is 0.05 For EX3

REFERENCES

[1] G. E. Forsythe, W. R. Wasow, Finite difference method for partial differential equations, Cambridge University Press, New York, Wiley, 1960.

[2] A. A. Samarskii, P. N. Vabishchevish, L. G. Vulkov, Finite difference methods: Theory and Applications, Nova Science Publishers, New York, 1999.

[3] Courant R, Variational methods for the solution of problems of equilibrium and vibrations, Bulletin of American Mathematical Society, 1943, 49, 1–23.

[4] Clough R W. Thoughts about the origin of the finite element method. Computers and Structures, 2001, 79:2029–2030.

[5] Clough R W. Early history of the finite element method from the view point of a pioneer, International Journal for Numerical Methods in Engineering. 2004, 60:283–287.

[6] Susanne C. Brenner, L. Ridgway Scoot, The mathematical theory of finite element method, Spring Science Business Media. 2008.

[7] G. R. Liu, S. S. Quek, The finite element method: A practical Course, Butterworth Heinemann, Oxford, 2003.

[8] G. R. Liu, M. B. Liu, Smoothed Particle Hydrodynamics- A meshfree Practical Method, World Science, Singapore, 2003.

[9] B. Nayroles, G. Touzot, P. Villon, Generalizing the finite element method: diffuse approximation and diffuse elements, Computational Mechanic, 10, 307–318, 1992.

[10] Y. Belytschko, Y. Y.Lu, L. Gu, Element-free Galerkin method, International Journal for Numerical Methods in Engineering, 20, 229–256, 1994.

[11] W. K. Liu, S. Jun, Y. F. Zhang, Reproducing kernel particle methods, International Journal for Numerical Method in Engineering, 20, 1081–1106, 1995.

[12] S. N. Atluri, T. Zhu, A new meshless local Petrov-Galerkin (MLPG) approach in computational mechanics, Computational Mechanics, 22, 117–127, 1998.

[13] P. Tongsuk, W. Kanok-Nukulchai, Further investigation of element-free Galerkin method using moving kriging interpolation, International Journal of Computational Methods, 1, 345–365, 2004.

[14] G.R . Liu, Meshfree Method: Moving Beyond the Finite Element Method, CRC Press, Boca Raton, USA, 2002 (1st Edn), 2009 (2nd Edn).

[15] J. S. Chen, C. T. Wu, S Yoon, Y You, A stabilized conforming nodal integration for Galeikin meshfree methods, International Journal for Numerical Method in Engineering, 50, 435–466, 2001.

[16] G. R. Liu. A G space theory and a weakened weak (W2) form for a unified formulation of compatible and incompatible methods: Part I theory. Int. J. Numer. Meth. Engng 2010.

[17] G. R. Liu. A G space theory and a weakened weak (W2) form for a unified formulation of compatible and incompatible methods: Part II theory. Int. J. Numer. Meth. Engng 2010.

[18] G. R. Liu, G. Y. Zhang, Y. Y. Wang, Z. H. Zhong, G. Y. Li, X. Han, A linearly conforming point interpolation method (LC-PIM) for 2D solid mechanics problems, International Journal of Computational method, 2, 645–665, 2005.

[19] G. R. Liu, T. Nguyen-Thoi, K. Y. Lam, Theoretical aspects of the smoothed finite element method (SFEM), International Journal for Numerical Methods in Engineering, 71, 902–930, 2007.

[20] G. R. Liu, T. Nguyen-Thoi, X. H. Nguyen, K. Y. Lam, A node-based smoothed finite element method(N-SFEM) for upper bound solution to solid mechanics problems, Computers and Structures, 87, 14–26, 2009.

[21] G. R. Liu, T. Nguyen-Thoi, X. H. Nguyen, K. Y. Lam, An edge-based smoothed finite element method (E-SFEM) for static, free, and forced vibration analysis, Journal of Sound and Vibration, 320, 1100–1130, 2009.

[22] G. R. Liu, G. Y. Zhang, Upper bound solution to elasticity problems: a unique property of the linearly conforming point interpolation method (LC-PIM), International Journal for Numerical Methods in Engneering, 74, 1128–1161, 2008.

[23] G. R. Liu, Nguyen Thoi Trung, Smoothed Finite Element Method, CRC press, 2010.

[24] S. C. Wu, G. R. Liu, H. O. Zhang, G. Y. Zhang, A node-based point interpolation method (NS-PIM) for thermo elastic problems with solution bounds, International journal of heat and mass transfer, 52, 1464–1471, 2009.

[25] G. R. Liu, G. Y. Zhang, Edge-based smoothed point interpolation methods, International journal of computational methods, 5, 621–646, 2008.

[26] G. rR. Liu, G. rY. Zhang, A normal G space and weakened weak (W2) formulation of a cell-based smoothed point interpolation method, International journal of computational methos, 6, 147–179, 2009.

[27] Kansa, Edward J, Multiquadrics – A scattered data approximation scheme with applications to computational fluid-dynamics – I surface approximations and partial derivative estimates, Computers & Mathematics with applications, 19(1990), no.8, 127–145.

[28] Kansa, Edward J, Multiquadrics – A scattered data approximation scheme with applications to computational fluid-dynamics – II solutions to parabolic, hyperbolic and elliptic partial differential equations, Computers & Mathematics with applications, 19(1990), no.8-9, 147–161.

[29] G. R. Liu, G. Y. Zhang, Smoothed Point Interpolation Methods, World Scientific Publishing, 2013.

[30] M. Chen, M. Li, G. R. Liu, Mathematic basis of G space, 2016.

[31] Liu, G. R., A Generalized Gradient Smoothing Technique and the Smoothed Bilinear Form for Galerkin Formulation of a Wide Class of Computational Methods, International Journal of Computational Methods, vol. 5, no. 2, pp. 199–236, 2008.

[32] Liu, G. R., An Overview on Meshfree Methods: For Computational Solid Mechanics, International Journal of Computational Methods, Vol. 13, No. 5, 2016.

[33] E. Larsson, E. Lehto, A. Heryudono, B. Fornberg, Stable computing of differentiation matrices and scattered node stencils based on Gaussian radial basis functions, SIAM Journal on Scientific Computing, Vol. 35, No. 4, 2013.